N91-17087

COMPARISON AND TESTING OF EXTENDED KALMAN FILTERS FOR ATTITUDE ESTIMATION OF THE EARTH RADIATION BUDGET SATELLITE

by

Julie Deutschmann
Flight Dynamics Analysis Branch
NASA Goddard Space Flight Center
Greenbelt, MD 20771

Itzhack Y. Bar-Itzhack
Aerospace Department
Technion-Israel Institute of Technology
Haifa 32000 Israel

Mohammad Rokni
Computer Sciences Corporation
Lanham-Seabrook, MD 20706

ABSTRACT

This paper presents the testing and comparison of two Extended Kalman Filters (EKFs) developed for the Earth Radiation Budget Satellite (ERBS). One EKF updates the attitude quaternion using a four component additive error quaternion . This technique is compared to that of a second EKF, which uses a multiplicative error quaternion. A brief development of the multiplicative algorithm is included. The mathematical development of the additive EKF was presented in the 1989 Flight Mechanics/Estimation Theory Symposium along with some preliminary testing results using real spacecraft data. A summary of the additive EKF algorithm is included. The convergence properties, singularity problems, and normalization techniques of the two filters are addressed. Both filters are tested with simulated ERBS sensor data in addition to real ERBS sensor data. The results of the two filters are also compared to those from the ERBS operational ground support software, which uses a batch differential correction algorithm to estimate attitude and gyro biases. Sensitivity studies are performed on the estimation of sensor calibration states. The potential application of the EKF for real time and non-real time ground attitude determination and sensor calibration for future missions such as the Gamma Ray Observatory (GRO) and the Small Explorer Mission (SMEX) is also presented.

I. INTRODUCTION

The purpose of this study was to test and compare two EKFs developed for ERBS. ERBS is equipped with the following sensors that are used for attitude determination: 2 redundant Inertial Reference Units (IRUs) each containing 3 single-axis gyroscopes, 2 digital fine Sun sensors (FSSs), 2 infrared (IR) horizon scanners, and 1 three-axis magnetometer. The state estimated by both EKFs consists of the attitude parameters, sensor misalignments for the Sun sensor, magnetometer and gyros, biases for the Sun sensor, horizon scanner, magnetometer and gyros, and scale factors for the Sun sensor, horizon scanner, magnetometer and gyros. A real time EKF was also developed which estimates only the attitude parameters and the gyro bias.

The development and initial testing of the additive EKF was presented in Reference 1. This filter was tested with only real data over short timespans. A multiplicative EKF was designed and tested and is presented in Reference 2. This work presents further testing of the additive EKF and comparison of the additive EKF to a multiplicative EKF adapted from that presented in Reference 2. The two filters are also compared, when possible, to the current ERBS batch algorithm which is used for fine attitude and gyro bias estimation. Both simulated data and real data are used for the testing and comparison.

In the additive EKF, the estimated quaternion is not necessarily normal unless it converges to the correct quaternion. Reference 3 shows that normalization speeds convergence of the filter and eliminates the need for filter tuning. The normalization techniques used in References 1 and 3 were external to the EKF algorithm. The covariance computation was not affected by the normalization, but the state estimation algorithm had to be modified to incorporate the part of the state estimate that was lost in the normalization. The realization of the normalization process as an update using a pseudo-measurement blends naturally into the EKF algorithm and does not require any modification of the EKF itself. This technique is tested on the additive EKF and compared to the original normalization process. The need for normalization in the multiplicative EKF is also presented.

II. THE EXTENDED KALMAN FILTER ALGORITHM

The EKF algorithm is based on the following assumed models

System model

$$\dot{\underline{X}} = \underline{f}(\underline{X}(t),t) + \underline{w}(t) \qquad (2.1)$$

Measurement model

$$\underline{z}_k = \underline{h}_k(\underline{X}(t_k)) + \underline{v}_k \qquad (2.2)$$

where: $\underline{X}(t)$ = state vector
$\underline{w}(t)$ = zero mean white process
$\underline{v}_k$ = zero mean white sequence

The measurement update and the propagation of the state estimate and of the error covariance are performed as

Update:
$$\hat{\underline{X}}_k(+) = \hat{\underline{X}}_k(-) + K_k[\underline{z}_k - \underline{h}_k(\hat{\underline{X}}_k(-))] \qquad (2.3)$$

where the gain matrix, K, is evaluated as

$$P_k(+) = [I - K_kH_k]P_k(-)[I - K_kH_k]^T + K_kR_kK_k^T \qquad (2.4)$$

$$K_k = P_k(-)H_k^T(\hat{\underline{X}}_k(-))[H_k(\hat{\underline{X}}_k(-))P_k(-)H_k^T(\hat{\underline{X}}_k(-)) + R_k]^{-1} \qquad (2.5)$$

Propagation:

$$\dot{\hat{\underline{X}}}(t) = \underline{f}(\hat{\underline{X}}(t),t) \qquad (2.6)$$

$$\dot{P}(t) = F(\hat{\underline{X}}(t),t)P(t) + P(t)F^T(\hat{\underline{X}}(t),t) + Q(t) \qquad (2.7)$$

where:

$$F(\underline{X}(t),t) = \left.\frac{\underline{f}(\underline{X}(t),t)}{\underline{X}(t)}\right|_{\underline{X}(t)=\hat{\underline{X}}(t)} \qquad (2.8a)$$

$$H(\underline{X}(-)) = \left.\frac{\underline{h}(\underline{X}(t))}{\underline{X}(t)}\right|_{\underline{X}(t)=\hat{\underline{X}}} \qquad (2.8b)$$

P_k = estimation error covariance matrix
R_k = covariance matrix of the white sequence $\underline{v}_k$
Q_k = spectral density matrix of $\underline{w}(t)$

The state vector was selected to be

$$\underline{X} = \begin{bmatrix} \underline{q} \\ \underline{S}_g \\ \underline{\Theta}_g \\ \underline{b}_g \\ \underline{\Theta}_s \\ \underline{S}_s \\ \underline{b}_s \\ \underline{b}_h \\ \underline{S}_m \\ \underline{\Theta}_m \\ \underline{b}_m \end{bmatrix} \qquad (2.9)$$

$\underline{q}$	4 quaternion components
$\underline{S}_g$	3 gyro scale factor errors
$\underline{\Theta}_g$	6 gyro misalignment angles
$\underline{b}_g$	3 gyro biases
$\underline{\Theta}_s$	3 FSS misalignment angles
$\underline{S}_s$	2 FSS scale factor errors
$\underline{b}_s$	2 FSS biases
$\underline{b}_h$	2 IR horizon scanner biases
$\underline{S}_m$	3 magnetometer scale factor errors
$\underline{\Theta}_m$	6 magnetometer misalignments
$\underline{b}_m$	3 magnetometer biases

The effective measurements used to update the filter are defined as

$$\underline{Y} = M_{AT}\underline{W}_{T',meas} - A(\hat{\underline{q}})\underline{V}_I \qquad (2.10)$$

where: $\underline{Y}$ = effective measurements (or residuals)
M_{AT} = transformation matrix from nominal (nonmisaligned) sensor to body coordinates
$\underline{W}_{T',meas}$ = unit vector as measured by the sensor in the sensor misaligned coordinates

$\hat{A}(\underline{g})$ = transformation matrix from inertial to body coordinates as a function of the estimated quaternion

$\underline{V}_I$ = measured unit vector as known in inertial coordinates

While the traditional EKF algorithm updates the state estimate according to (2.3), we use $\underline{y}$ (as computed in (2.10)) to update the state estimate as

$$\hat{\underline{X}}_k(+) = \hat{\underline{X}}_k(-) + \underline{x}(t_k) \qquad (2.11) \qquad \text{where:} \quad \underline{x}(t_k) = K_k \underline{y}_k \qquad (2.12)$$

It can then be shown (Reference 1) that $\underline{z}_k - \underline{h}_k(\hat{\underline{X}}_k(-))$ is linearly related to $\underline{x}(t_k)$. The EKF estimates $\underline{x}(t_k)$ and then adds the estimate $\underline{x}(t_k)$ to $\hat{\underline{X}}_k(-)$, the best estimate of $\underline{X}(t_k)$. The linear relationship between $\underline{x}(t_k)$ and $\underline{y}_k$ will be shown in Section IV.

In the additive EKF, the first four components of $\underline{x}(t_k)$ are the corrections to the quaternion estimated by the EKF, denoted as $\delta\underline{g}$. These corrections are added to $\underline{g}(-)$, the best estimate of $\underline{g}$. The remaining elements in $\underline{x}(t_k)$ are the corrections to the calibration states which are also then added to the current best estimate of those states.

In the multiplicative EKF, the quaternion elements of $\underline{x}(t_k)$ are treated differently. The definition of $\underline{x}(t_k)$ is given as

$$\underline{x}(t_k) = \begin{bmatrix} \underline{\alpha} \\ \underline{\delta\tau} \end{bmatrix} \qquad (2.13)$$

where:

$\underline{\alpha} = \begin{bmatrix} \phi \\ \Omega \\ \mu \end{bmatrix}$ = three small angles based on the assumption that the error quaternion is composed of three small angles (as the vector portion) and 1 (scalar portion)

$\underline{\delta\tau}$ = corrections to the calibration parameters given in (2.9)

The correction to the quaternion, given as $\delta\hat{\underline{g}}$, is then constructed according to

$$\delta\hat{\underline{g}}^T = \begin{bmatrix} \tfrac{1}{2}\phi & \tfrac{1}{2}\Omega & \tfrac{1}{2}\mu & 1 \end{bmatrix} \qquad (2.14)$$

The quaternion is updated as

$$\hat{\underline{g}}_{k+1}(+) = \hat{\underline{g}}_{k+1}(-)\delta\hat{\underline{g}}^{-1} \qquad (2.15)$$

The calibration components are updated according to (2.11). The updated values of the calibration components and $\hat{\underline{g}}_{k+1}(+)$ are augmented into (2.9) and are propagated in time using (2.6). The dynamics of the two EKFs will be presented in the next section. For further discussion of the algorithms see References 1 and 2.

III. THE DYNAMICS MODEL

The states that vary in time are the attitude parameters and "bias" states that are modeled as Markov rather than true bias states. The scale factors and misalignments are assumed to be constant in time. The elements of $\underline{x}(t_k)$ for the additive filter are the same as those shown in (2.9) with the quaternion error, $\delta\underline{g}$, replacing $\underline{g}$. The differential equation which governs the propagation of $\underline{x}$ is obtained by combining the linear differential equations of the components of the attitude augmented state vector. This yields an equation of the form

$$\dot{\underline{x}} = F(\hat{\underline{X}})\underline{x} + \underline{n} \qquad (3.1)$$

This equation is presented below with F and $\underline{n}$ given. The matrices $\tilde{\Phi}$, $\hat{B}$, $\tilde{U}$, $\tilde{W}$, and T which form F are derived and defined in Reference 1. F given below and in (3.1) is defined in (2.8a). It is used to propagate the covariance matrix in (2.7).

$$\frac{d}{dt}\begin{bmatrix} \delta\underline{x} \\ \underline{s}_g \\ \underline{\theta}_g \\ \underline{b}_g \\ \underline{\theta}_s \\ \underline{s}_s \\ \underline{b}_s \\ \underline{b}_h \\ \underline{s}_m \\ \underline{\theta}_m \\ \underline{b}_m \end{bmatrix} = \begin{bmatrix} \tilde{\Phi} & \hat{B}\tilde{U} & \hat{B}\tilde{W} & \hat{B} & & & & & & & \\ & & & T_g & & & & & & & \\ & & & & T_s & & & & & & \\ & & & & & T_h & & & & & \\ & & & & & & & & & T_m & \end{bmatrix} \begin{bmatrix} \delta\underline{x} \\ \underline{s}_g \\ \underline{\theta}_g \\ \underline{b}_g \\ \underline{\theta}_s \\ \underline{s}_s \\ \underline{b}_s \\ \underline{b}_h \\ \underline{s}_m \\ \underline{\theta}_m \\ \underline{b}_m \end{bmatrix} + \begin{bmatrix} \hat{B}\underline{n}_{g1} \\ \\ \underline{n}_{g1} \\ \\ \\ \underline{n}_s \\ \underline{n}_h \\ \\ \\ \underline{n}_m \end{bmatrix} \qquad (3.2)$$

In the multiplicative EKF, $\underline{x}$ is replaced with (2.13) and the first row of $F(\underline{X})$ is replaced with

$$\begin{bmatrix} \tilde{\Omega} & -\tilde{U} & \tilde{W} & I & & & & & & & \end{bmatrix} \qquad (3.3)$$

where:

$$\tilde{\Omega} = \begin{bmatrix} 0 & \tilde{w}_z & -\tilde{w}_y \\ -\tilde{w}_z & 0 & \tilde{w}_x \\ \tilde{w}_y & -\tilde{w}_x & 0 \end{bmatrix} \qquad (3.4)$$

I = 3x3 identity matrix

The first row of $\underline{n}$ in (3.1), defined in (3.2), is replaced by $\underline{n}_{g1}$. The spectral density of the elements of the white noise driving the Markov states in $\underline{x}$ in both EKFs is related to the individual states they drive according to the well known relation $Q_i = 2\sigma^2_{i,o}/T_i$ (Reference 4) where Q_i is the spectral density of the white noise driving state i, T_i is the time constant of this Markov state and $\sigma_{i,o}$ is the initial standard deviation of the state.

The estimation problem dealt with in this paper is characterized by a linear dynamics equation. The system dynamics can be augmented to obtain an equation of the form (Reference 1)

$$\dot{\underline{X}} = f(t)\underline{X} + \underline{n} \qquad (3.5)$$

where $\underline{X}$ is given in (2.9) (for both EKFs) and the first row of F(t) in (3.2) is replaced with the following to define f(t)

$$\begin{bmatrix} \tilde{\Phi} & & & & & & & & & & \end{bmatrix} \qquad (3.6)$$

The white noise vector $\underline{n}$ in (3.5) is of no consequence in the estimation process since according to (2.6) the propagation of $\underline{X}$ requires only the evaluation of f(t).

IV. THE MEASUREMENT MODEL

As mentioned in Section II the effective measurements used to update the filter are defined as

$$\underline{y} = M_{AT}\underline{W}_{T',meas} - A(\hat{\underline{g}})\underline{V}_I \qquad (4.1)$$

Incorporating the sensor misalignments, scale factor errors, and biases into (4.1) the linear relationship between $\underline{y}$ and $\underline{x}$ can be derived. This yields the following

$$\underline{y} = H_q d\underline{g} + M_{AT}[\underline{W}_{T',meas}^{x}]\underline{\theta} + M_{AT}d\underline{W}_{T'} \qquad (4.2)$$

The terms introduced in (4.2) are derived and defined in Reference 1. The term $[\underline{W}_{T'},_{meas}x]$ represents the replacement of the cross product with the multiplication of an anti-symmetric matrix, composed of $\underline{W}_{T'},_{meas}$. Equation (4.1) shows how to generate the effective measurement $\underline{y}$ which updates the estimate and (4.2) indicates the linear relationship between $\underline{y}$, the attitude errors, the misalignment errors of the sensor being used and $d\underline{W}_{T'}$, the total error generated by the sensor. Equation (4.2) is the first stage in finding the measurement matrix, H, (defined in (2.8b)) for each sensor used onboard ERBS.

The effective measurement (4.1) for the multiplicative EKF is computed in the same manner with A_{CI} replacing $A(\underline{q})$. A_{CI} is the transformation from the inertial to the computed (estimated) body orientation. The first term of (4.1) is manipulated the same as in Reference 1, but the second term is expanded in a different manner. This process is outlined below. The matrix A_{CI} can be written as

$$A_{CI} = A_{CA}A_{AI} \qquad (4.3)$$

where: A_{CA} = transformation matrix from the true body to the estimated body system
A_{AI} = transformation matrix from the inertial to the true body system

The matrix A_{CA} can be written as

$$A_{CA} = I - [\underline{\alpha}x] \qquad (4.4)$$

where $\underline{\alpha}$ are defined in (2.13). Using (4.4) in (4.3) gives

$$A_{CI} = (I - [\underline{\alpha}x])A_{AI} \qquad (4.5)$$

Substituting (4.5) into (4.1) with the expansion of the first term of (4.1) from Reference 1 gives

$$\underline{y} = [\underline{\alpha}x]A_{AI}\underline{V}_I - M_{AT}[\underline{W}_{T'},_{meas}x]\underline{\theta} + M_{AT}d\underline{W}_{T'} \qquad (4.6)$$

Note that $\underline{V}_A = A_{AI}\underline{V}_I$ but since we don't know A_{AI} we use the estimated matrix, i.e. $\underline{V}_c = A_{CI}\underline{V}_I$, therefore we can write (4.6) as

$$\underline{y} = [-\underline{V}_c x]\underline{\alpha} - M_{AT}[\underline{W}_{T'},_{meas}x]\underline{\theta} + M_{AT}d\underline{W}_{T'} \qquad (4.7)$$

The models for each of the sensors will now be given. From these models, the H matrix for each sensor is obtained. The derivation is shown in Reference 1.

FSS:

$$\underline{y} = \left[\begin{array}{c|c|c|c|c|c} & 0 \ldots 0 & & & & 0 \ldots 0 \\ H_q & 0 \ldots 0 & M_{AT}[\underline{W}_{T'},_{meas}x] & M_{AT}W_s & \begin{matrix}\tan A & 0 \\ 0 & \tan B\end{matrix} & M_{AT}W_s \\ & 0 \ldots 0 & & & & 0 \ldots 0 \end{array}\right] \underline{x} + M_{AT}W_s \begin{bmatrix} n_A \\ n_B \end{bmatrix} \qquad (4.8)$$

IR:

$$\underline{y} = \left[\begin{array}{c|c|c|c} & 0 \ldots 0 & & 0 \ldots 0 \\ H_q & 0 \ldots 0 & W_h & 0 \ldots 0 \\ & 0 \ldots 0 & & 0 \ldots 0 \end{array}\right] \underline{x} + W_h \begin{bmatrix} n_{hr} \\ n_{hp} \end{bmatrix} \qquad (4.9)$$

Magnetometer:

$$\underline{y} = \left[\begin{array}{c|c|c} & 0 \ldots\ldots\ldots 0 & \\ H_q & 0 \ldots\ldots\ldots 0 & M_{AT}B' \\ & 0 \ldots\ldots\ldots 0 & \end{array}\right] \underline{x} + W_h \begin{bmatrix} n_{xm} \\ n_{ym} \\ n_{zm} \end{bmatrix} \qquad (4.10)$$

In 4.8, 4.9, and 4.10 $[-\underline{V}_c x]$ replaces H_q in the multiplicative filter.

V. QUATERNION NORMALIZATION

The quaternion that represents attitude is normal. Reference 3 shows that forcing normalization on the

estimated quaternion is advantageous since it speeds up convergence and eliminates the need for filter tuning. Reference 1 describes the forced normalization of the additive filter. That normalization technique is equivalent to removing a portion of the estimate. That method of normalization is external to the EKF algorithm. A new normalization method was derived that blends naturally into the Kalman filter algorithm. The idea is to use the normalized quaternion as a "pseudo-measurement". Performing a measurement update with very small noise (ideally zero) on the "measurement" then pushes the quaternion portion of the state to be the normalized quaternion. The algorithm is

$$\underline{z} = \frac{\hat{\underline{q}}_k(+)}{|\hat{\underline{q}}_k(+)|} \qquad (5.1) \qquad \text{where:} \quad \hat{\underline{q}}_k(+) = \text{the upper four elements of } \hat{\underline{X}}_k \text{ in (2.9)}$$

The "measurement" covariance matrix can then be defined as:

$$R = \begin{bmatrix} 1 & 0 & 0 & 0 \\ 0 & 1 & 0 & 0 \\ 0 & 0 & 1 & 0 \\ 0 & 0 & 0 & 1 \end{bmatrix} \delta \qquad (5.2) \qquad \text{where:} \quad \delta = \text{a very small dimensionless number}$$

The measurement matrix, H, is defined as

$$H = \left[\begin{array}{cccc|ccc} 1 & 0 & 0 & 0 & 0 & \cdots & 0 \\ 0 & 1 & 0 & 0 & 0 & \cdots & 0 \\ 0 & 0 & 1 & 0 & 0 & \cdots & 0 \\ 0 & 0 & 0 & 1 & 0 & \cdots & 0 \end{array}\right] \qquad (5.3)$$

The gain is computed according to (2.4). The state is updated as

$$\hat{\underline{X}}_k^*(+) = \hat{\underline{X}}_k(+) + K[\underline{z} - H\hat{\underline{X}}(+)] \qquad (5.4)$$

The covariance is updated with (2.5). This measurement update process is according to a linear Kalman filter and not the extended Kalman filter since it handles the state $\underline{X}$ directly in the update and not the error state, $\underline{x}$.

The quaternion is also normalized in the multiplicative EKF for the same reasons as the additive EKF. The normalization process used was a forced normalization. The quaternion was simply normalized with no compensation performed.

VI. COMPENSATION

When propagating the state estimate and the covariance, we use the measured angular velocity. We know, however, that the propagated values are not accurate because the gyro output contains errors. We can better estimate those errors if we correct the gyro output for estimated errors. This operation is known as calibration.

We also want to compensate the measurements obtained from the FSS, the IR horizon scanner, and the magnetometers which are all orientation measuring devices whose output are used to update the filter. The reason we want to compensate the output from these sensors is different in nature than the reason for compensating the gyro output. In (2.11) we estimate the difference between the true value of $\underline{X}$ and its latest estimate, and add the estimate of the difference to the latest estimate of $\underline{X}$ to form its updated estimate. Let us consider an error term in one of the sensor measurements (say a bias). This bias is a part of $\underline{W}_{T',meas}$ and, thus, as indicated in (4.1) bears its signature on $\underline{y}$. Consequently, if certain observability conditions are met, it is estimated and added to the state estimate as indicated in (2.11). If no compensation takes place, the next time the measurements of this sensor are processed the bias is again estimated and added to the previous estimate of this bias, thus creating an estimate that is too large and incorrect. The proper way to handle this case is to eliminate the estimate of the bias from $\underline{W}_{T',meas}$ so that only the residual bias, which has not been estimated yet, is present in $\underline{y}$ as shown in (4.1). Only the

estimate of this residual is added to the existing estimate of the bias, which is a part of $\hat{X}$, yielding a correction to the previous estimate. This logic holds for the other error states, too. Reference 1 outlines this method. The compensation was applied to the multiplicative EKF in the same manner.

VII. SINGULARITIES

It was found that the models for both the additive and multiplicative EKFs presented in Section IV contain singularities. The IR and FSS measure only two quantities (direction). Artificial generation of a vector measurement based on the IR and FSS measurements constitutes a projection of two-dimensional information on a three dimensional space. Such projection yields a singular noise covariance matrix. Another singularity exists in the additive EKF. This is because only three parameters are necessary to specify attitude. Adding a fourth parameter results in the computation of HPH^T being singular.

To compensate for the first singularity, the noise covariance matrices for the FSS and IR were reduced to 2x2 matrices. This forced the elimination of the third row of H. Note that the magnetometer measures three independent components, and no alterations of its noise covariance and H matrices are necessary. In the additive EKF, the singularity of HPH^T is not removed by this operation. The nonsingular R keeps the computation of $(HPH^T + R)$ in equation (2.4) from becoming singular.

Several tests were run to verify that the singularities were eliminated. It was found that as the uncertainties in the measurement noises were reduced on the FSS and IR, the singular HPH^T in the additive EKF cannot be compensated for by the noise covariance matrices. The uncertainties in the FSS and IR measurement noises were kept at 0.01 degrees or higher to avoid this. It was found in the multiplicative EKF that near singular conditions can exist initially with a large initial attitude error. The filter overcomes the singularity as the state is updated. This singularity exists because the assumption given by (2.14), that the first three elements of δq are small, is violated.

VII. RESULTS

Several scenarios were run with both filters to study the characteristics of the two filters. Simulated data were used for most of the tests. The simulated data had an attitude solution of 0 degrees yaw, roll, and pitch. The x, y, and z gyro bias were approximately -1.7, 1.2, and 1.5 deg/hour during the first portion of the orbit. During the latter portion of the orbit when the FSS had coverage, the y bias was approximately -2.6 deg/hour for a short time period (around 200 seconds) and then it changed back to 1.2 deg/hour. (The y bias flipped in the simulated data due to the orbit eccentricity.) Other than the gyro bias the data were clean with no noise. Other sensor calibrations were studied by applying errors to the different sensors and seeing how well the two filters could estimate these errors. Real data were also used for some of the tests and the results will be presented after the simulated data test results. When possible, results from the batch estimator are also provided. The quaternion given in (2.9) defines the attitude in inertial coordinates. It was converted to geodetic pitch, roll, and yaw solutions for display and comparison to the batch solutions.

Simulated Data

The first study performed was a sensitivity study of the gyro bias to determine the best value for the a priori covariance. The a priori covariance was varied to determine what value gave the lowest error in the attitude and gyro bias solutions. As mentioned in Section III the gyro bias was modeled as a Markov process. It was found in this scenario that, since the bias does not change, both filters behaved better when the time constant on the Markov was set very high. This essentially models the bias as a constant. The time constant was set to $1x10^5$ seconds. The results of the sensitivity study showed that the best a priori value for the

Table 1. A Priori Values for Both Filters

Attitude - specified for run	P_o other states - 0 unless specified	FSS measurement σ- 0.01 degrees
Other states - 0	Q attitude - $2x10^{-9}$ rad²/sec²	IR measurement σ- 0.01 degrees
P_o attitude (quaternion) - 0.0625	Q Markov - see Section III	Magnetometer measurement
P_o gyro bias - $1x10^{-7}$ rad²/sec²	time constants - $1x10^5$ sec	σ- 3 milliGauss

gyro bias covariance was $\sigma^2=1x10^{-7}$ rad²/sec². All other a priori values are given in Table 1. These values were used in all runs except where noted.

The first case examined was a baseline case, solving only for attitude. The a priori attitude error was 50 degrees. Figures 1a and 1b show the yaw solutions from the additive EKF and batch algorithm. The multiplicative EKF yaw solution has the same shape as the additive EKF with the same final value. All three sensors were used in the estimation. Both filters show similar behavior, converging quickly. The batch solution converged onto the wrong solution. The a priori error of 50 degrees was too high. The filter pitch and roll solutions converge very quickly, reaching values of 0.008 deg for roll and -0.001 degrees for pitch (both filters). The batch epoch solution for roll was -2.8 degrees and 4.5 degrees for pitch. The sensor residuals for the two filter solutions were very small, but not for the batch due to the large error in the solution.

The next case involved adding the estimation of gyro bias to the baseline run. The attitude could not be given such a large error in order for the solutions to converge. The a priori error was set to 10 degrees (the limit was around 20 degrees). The yaw solutions for the two filters were similar to those shown in Figure 1. The batch algorithm converged for all angles with final values similar to the filters. The pitch and roll solutions also converge very quickly for the filters with nominal final results. Figures 2a and 2b show the estimation of the gyro bias for the two filters (in the span of data used the FSS had coverage so the y gyro bias was approximately -2.6 deg/hr). The batch epoch gyro bias solution is listed on the figure as well. The batch algorithm gives a slightly better estimate of the gyro bias. The filter, in general, needs more than 100 seconds (typically 200 or more) to converge to the gyro bias solution. After 200 seconds the additive and multiplicative filters give

Additive (deg/hr)	Multiplicative (deg/hr)	Batch (deg/hr)
x = -1.22	x = -1.54	x = -1.7
y = -1.71	y = -2.16	y = -2.6
z = 2.25	z = 1.40	z = 1.5

The multiplicative shows a little quicker convergence to the gyro bias solution. Both converge beyond 200 seconds and remain stable.

The next iteration in the baseline study examined the effects of normalization. The pseudo-measurement normalization technique outlined in Section V was implemented into the additive filter. It was found that it did not give good results when the noise covariance matrix was quite small. In this case the estimated quaternion was almost completely replaced by the normalized quaternion and the covariance matrix converged to a very small value. The filter then goes to the normalized quaternion with huge confidence but the normalized quaternion is not necessarily the correct quaternion. Table 2 shows the results at 100 seconds for various values of δ, the diagonal element of the noise covariance matrix (see Equation 5.2). Table 2 also gives the result from the baseline case above, starting with an a priori error of 10 degrees and estimating gyro bias. The pseudo-measurement normalization has the most effect on the pitch solution. As δ is decreased, the pitch solution eventually diverges beyond what is given in Table 2.

Table 2. Pseudo-Measurement Normalization Results for Different Noise Levels (A priori attitude = 10 degrees, gyro bias estimated)

δ	Yaw (deg)	Roll (deg)	Pitch (deg)
$1x10^{-5}$	0.0031	0.0077	-0.0073
$1x10^{-7}$	0.0030	0.0075	-0.0073
$1x10^{-9}$	0.00037	-0.0078	0.084
baseline	0.0039	0.0078	-0.00058

Another characteristic of the pseudo-measurement technique is the increased use of computer processing time. It took approximately 15 percent more computer time with the pseudo-measurement technique than the original technique to process 1000 seconds. (This is due to the inversion of a 4x4 matrix.) Normalization is not very critical for attitude determination in this scenario. The attitude solutions without normalization and with the pseudo-measurement normalization technique are similar to those in the baseline cases discussed above. Figures 3a, 3b, and 3c show the gyro bias estimates from the additive and multiplicative EKFs with no

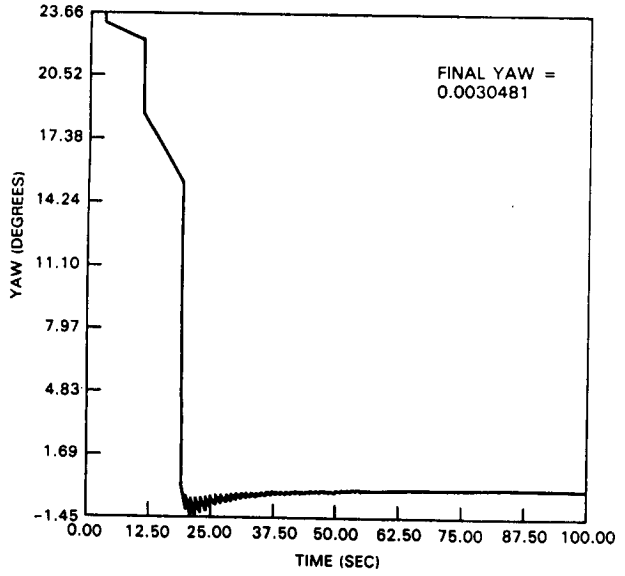

1a - ADDITIVE

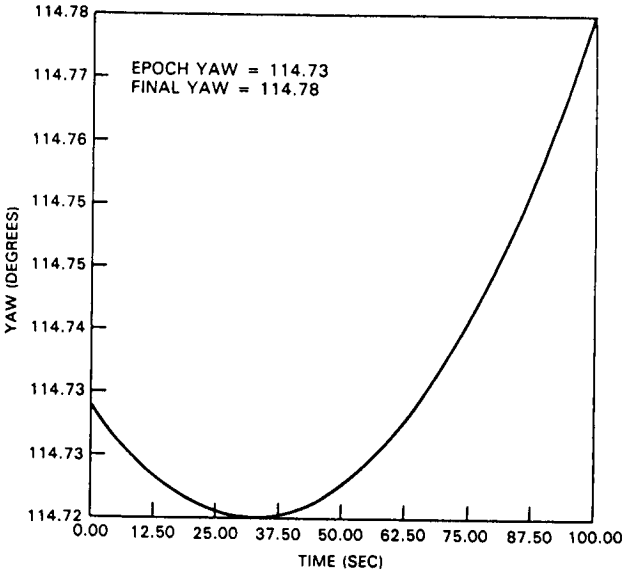

1b - BATCH

FIGURE 1. BASELINE YAW SOLUTIONS (APRIORI ATTITUDE = 50 DEG.)

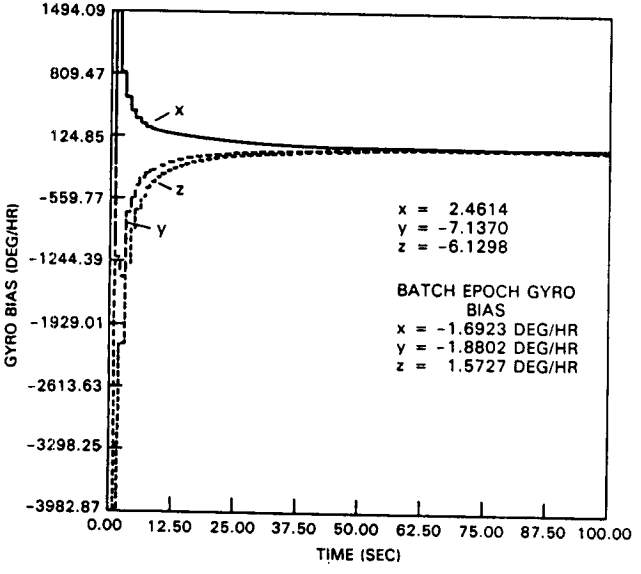

2a - ADDITIVE

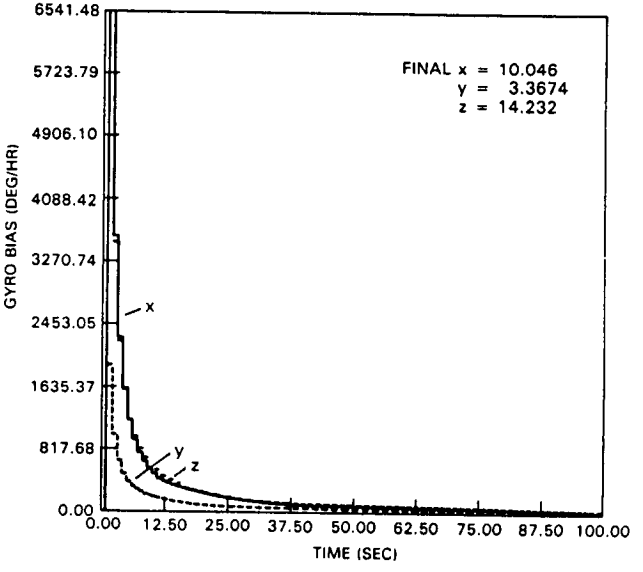

2b - MULTIPLICATIVE

FIGURE 2. GYRO BIAS ESTIMATE (APRIORI ATTITUDE = 10 DEG.)

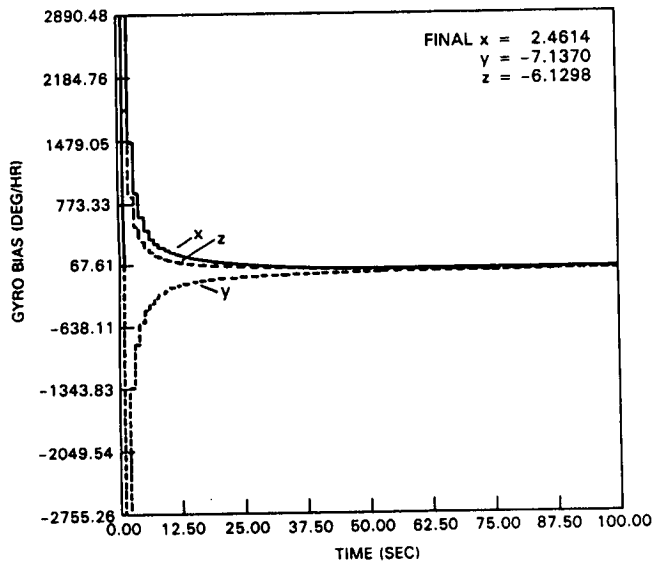

3a - ADDITIVE, NO NORMALIZATION

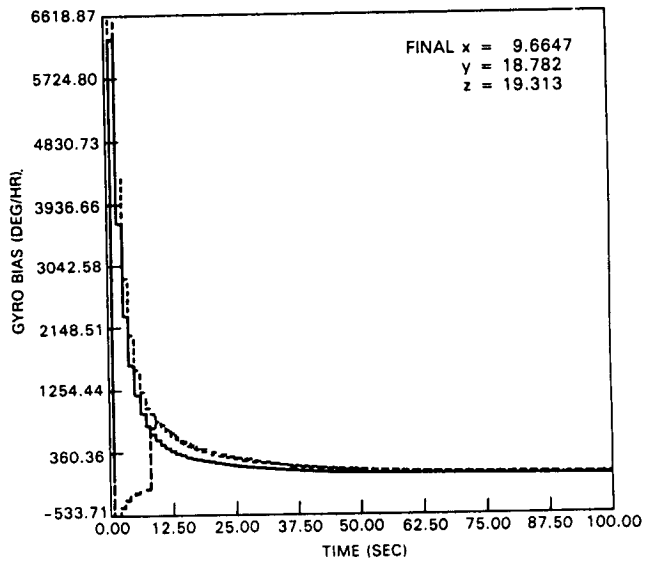

3b - MULTIPLICATIVE, NO NORMALIZATION

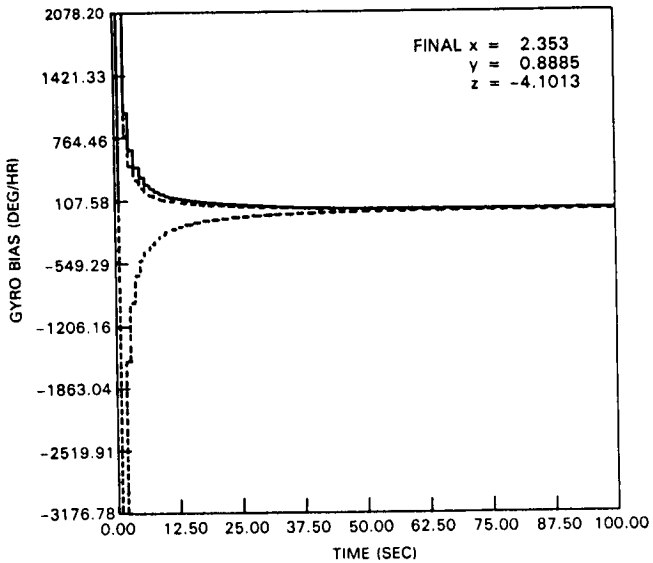

3c - ADDITIVE, PSUEDO-MEASUREMENT NORMALIZATION

FIGURE 3. GYRO BIAS ESTIMATES (APRIORI ATTITUDE = 10 DEG)

normalization and from the additive EKF with the pseudo-measurement normalization. The gyro bias is affected somewhat initially, but eventually the solutions converge. It was mentioned previously that Reference 3 shows normalization eliminates the need for filter tuning. Even though it is not crucial here it would be expected to have an effect similar to that found previously in other scenarios, perhaps cases that are not as nominal.

The next area examined was a yaw maneuver. The yaw was changed from 0 to 180 degrees at a constant rate. The gyro biases are different in this case. The values for x, y, and z start out with the original biases but after the maneuver they change to approximately 2.1, 1.2, and 1.6 deg/hr, respectively (due to geometry). Again attitude and gyro bias were estimated. This time an upper limit of 20 degrees initial attitude error was used. Figure 4a shows the yaw solution from the multiplicative EKF. The additive EKF and batch yaw estimates have the same shape with a final yaw values of 179.91 and 180.77 degrees. Both filter estimates and the batch estimate follow the maneuver very closely. The pitch and roll solutions exhibit nominal behavior and the residuals are extremely small. Figures 4b and 4c show the gyro bias estimates for both filters. After 100 seconds they have not quite converged due to the larger initial attitude error. At the end of the run (approximately 3000 seconds) the gyro bias has become quite stable with the values given below. The batch epoch gyro bias is also given below (using approximately 3000 seconds of data as well).

Additive (deg/hr)	Multiplicative (deg/hr)	Batch (deg/hr)
x = 1.712	x = 1.719	x = -0.442
y = 1.988	y = 1.467	y = 0.442
z = 1.446	z = 1.475	z = -0.050

The batch cannot follow a change in the gyro bias since it gives only one solution at the epoch. The solved for biases are influenced by the initial bias and the bias after the maneuver and thus are somewhat between the two.

In the following cases both filters were used to study the characteristics of using different sensor combinations, as opposed to using data from all three sensors concurrently. The combinations were IR/MAG, FSS/MAG, IR only, and MAG only. In all cases both filters showed poor estimation of gyro bias, particularly in those cases with magnetometer data. The magnetometer, which suffers from a digitization of 6 milliGauss, is too coarse to estimate gyro bias. This digitization results in the magnetometer having only coarse attitude estimation ability. Without the availability of a fine attitude solution the gyro bias is not observable.

Figures 5a and 5b show the estimation of yaw by the additive EKF and the batch algorithm for an IR/MAG combination. The multiplicative EKF yaw solution again had the same shape as the additive EKF with a final yaw of -0.664 degrees. The a priori attitude was set to 0 degrees and the gyro bias was estimated. All show similar values for attitude. It was found when using two sensors, one being the magnetometer, that better results were achieved when the FSS or IR measurement uncertainties were increased to 0.1 degrees. At 0.01 degrees there was too much disparity between the uncertainties and the filter exhibited more fluctuations. Figure 5c shows the gyro bias estimation from the additive EKF with the batch epoch solution listed. The multiplicative gyro bias estimates look like the additive with final x, y, and z values of -4.413, 0.852, and -2.090 deg/hr, respectively. The filter solutions show quite a bit of fluctuation. Between the three algorithms the final results are similar for x and y, but differ for z; the batch algorithm giving a much better estimate. The x value for all three algorithms and the z for the filters is not estimated very well due to the magnetometer inaccuracy. The batch algorithm also weights the sensors differently which could account for the differences in the final solution. The coarse estimation of yaw by the magnetometer (yaw is not observable in the IR sensor) is shown in Figure 5a. These errors corrupt the gyro bias solution. The pitch and roll behave nominally since they are estimated mainly by the IR sensor. The IR residuals are also very small. A sample of the magnetometer residual is also shown in Figure 5d. The digitization is apparent in the residual curve. Also shown are the expected values (plus and minus) of the residual (dashed lines). The magnetometer residual settles near these values.

An attempt was made to improve the gyro bias variation by increasing the uncertainty on the magnetometer from 3 to 50 milliGauss. This did not improve the results at all.

Without the gyro bias estimation, the IR/MAG solutions will converge from a much larger initial attitude error. Figures 5e and 5f show the yaw solutions for the multiplicative EKF and the batch algorithm with a 50 degree initial attitude error. The additive EKF yaw solution has the same shape as the multiplicative EKF with a final yaw of -0.123 degrees. All three algorithms have final solutions that are quite similar. The

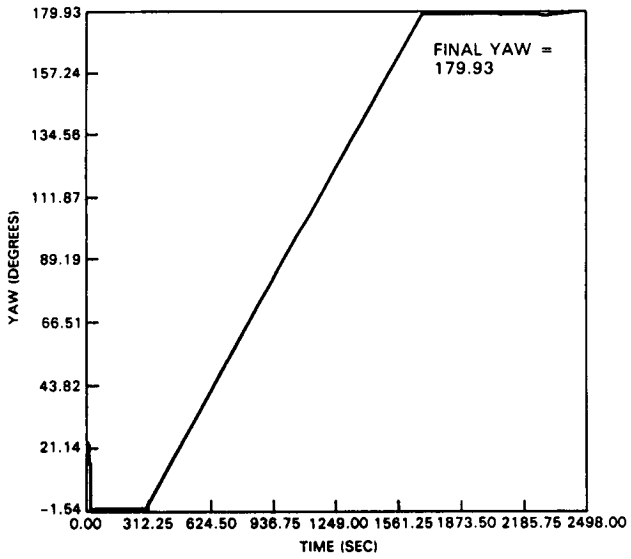

4a - YAW, MULTIPLICATIVE

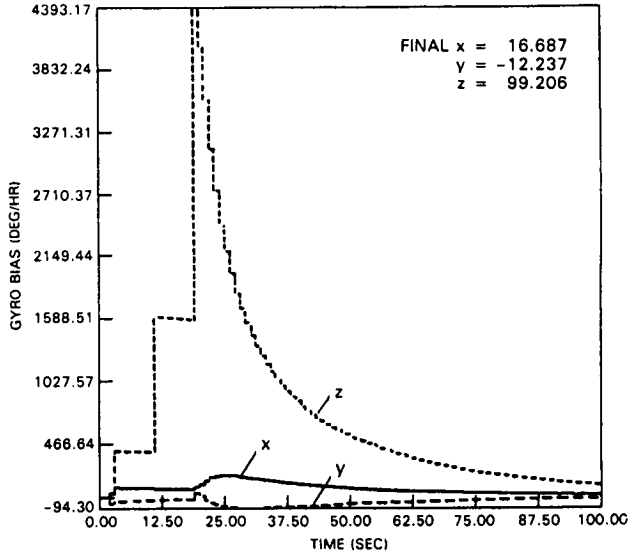

4b - GYRO BIAS, ADDITIVE

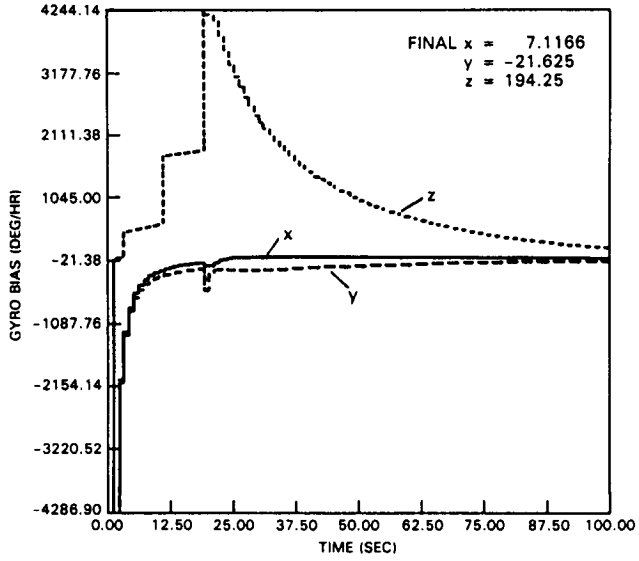

4c - GYRO BIAS, MULTIPLICATIVE

FIGURE 4. YAW MANEUVER (APRIORI ATTITUDE = 10 DEG)

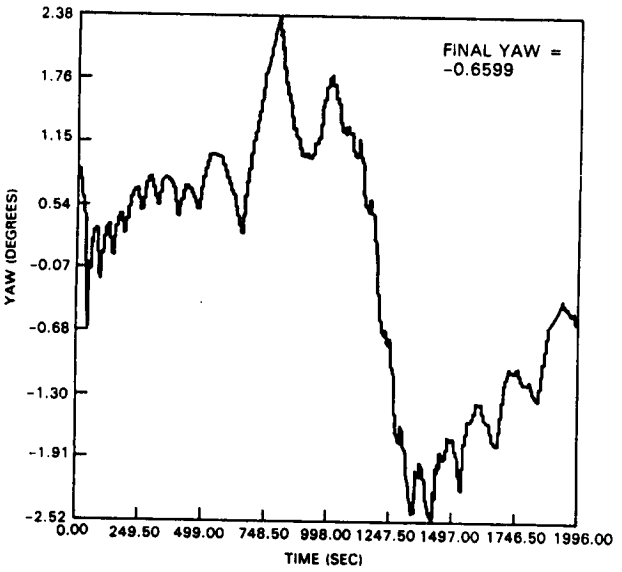

5a - YAW, ADDITIVE

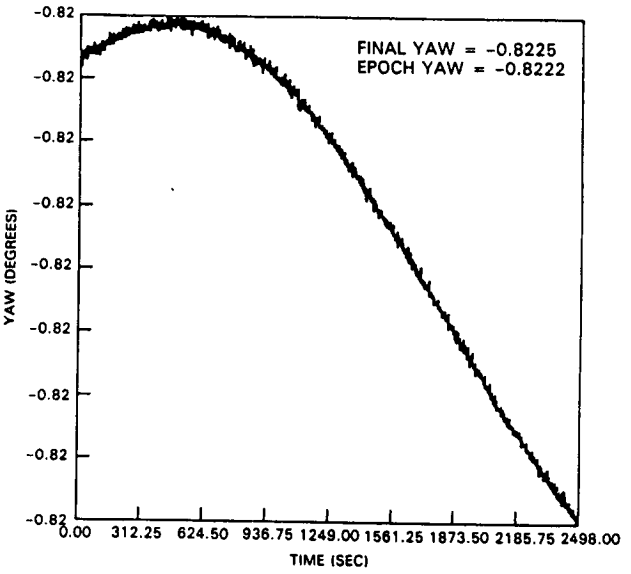

5b - YAW, BATCH

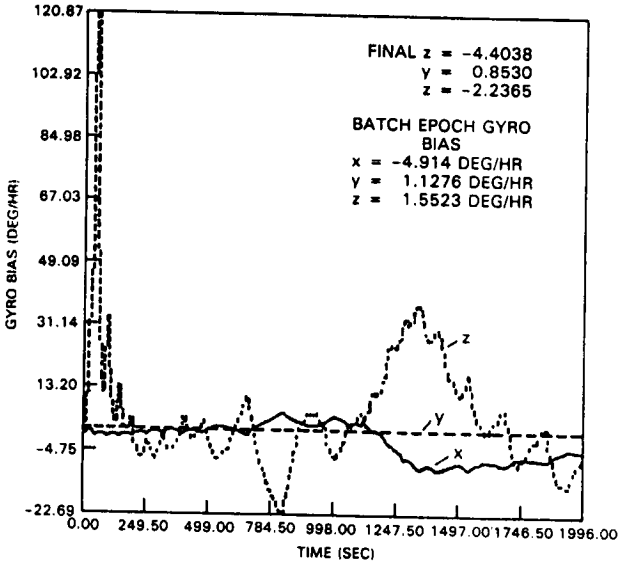

5c - GYRO BIAS, ADDITIVE

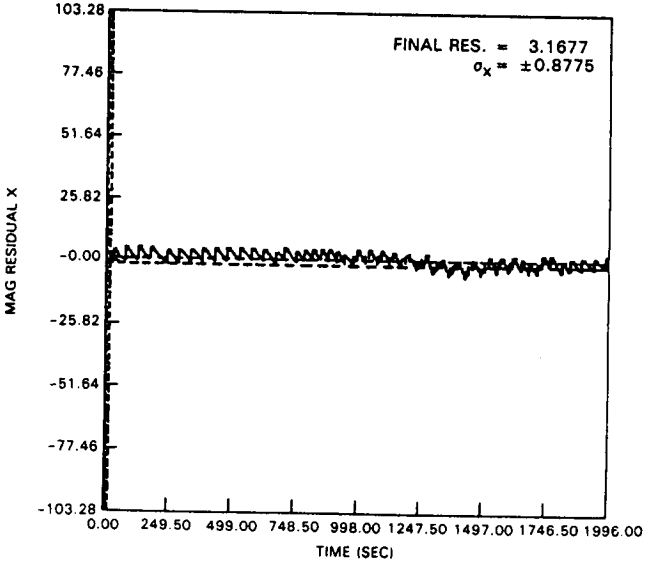

5d - MAGNETOMETER X RESIDUAL

FIGURE 5. IR/MAG SOLUTIONS (APRIORI ATTITUDE = 0 DEG)

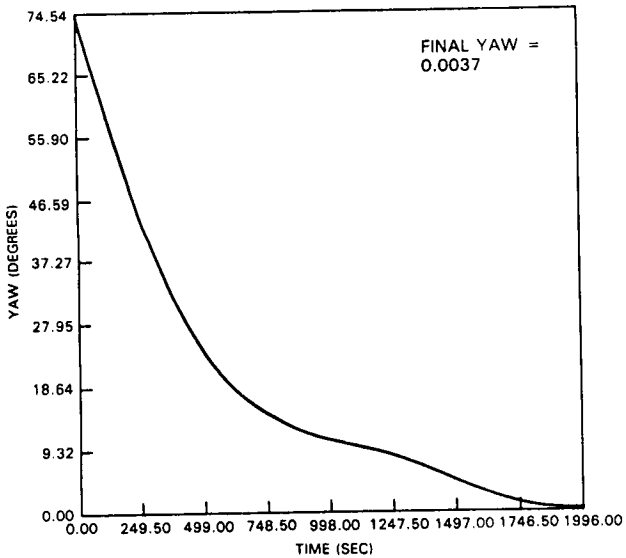

5e - YAW, MULTIPLICATIVE (APRIORI ATTITUDE = 50 DEG., NO GYRO BIAS)

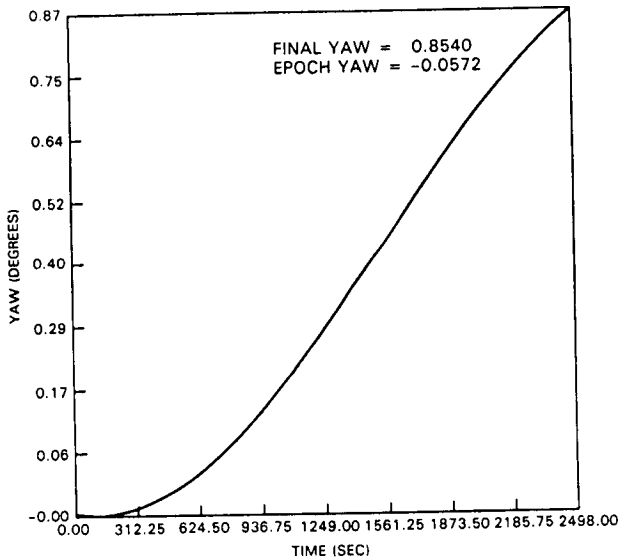

5f - YAW, BATCH (APRIORI ATTITUDE = 50 DEG., NO GYRO BIAS)

FIGURE 5. IR/MAG SOLUTIONS

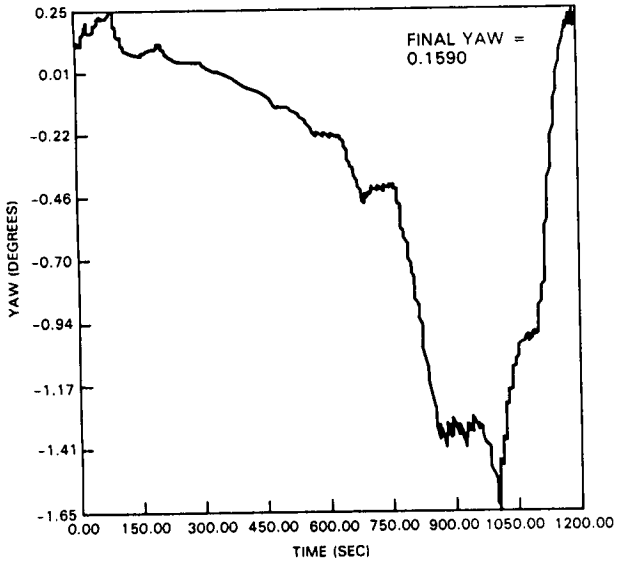

6a - YAW, ADDITIVE

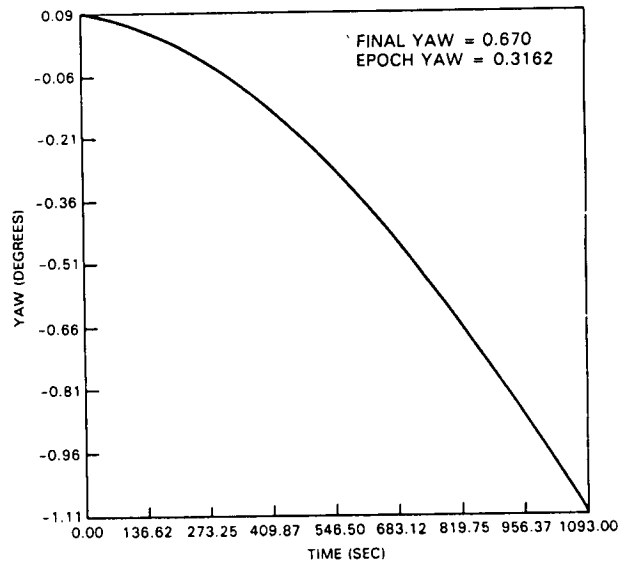

6b - YAW, BATCH

FIGURE 6. FSS/MAG SOLUTIONS (APRIORI ATTITUDE = 0 DEG)

pitch and roll solutions are nominal. The IR residuals are very small and the magnetometer residuals show similar behavior to that shown in Figure 5.d.

As in the IR/MAG case, solutions using an FSS/MAG combination were generated. Again the gyro bias was poorly estimated for the same reasons stated above. The algorithms were again started with a 0 degree initial attitude. Figures 6a and 6b show the additive EKF and the batch yaw solutions. The multiplicative EKF yaw solution again has the same shape as the additive but with a final yaw of 0.162 degrees. Both filter solutions exhibit quite a lot of fluctuation. The FSS loses coverage at 980 seconds. This causes more divergence in the solution. The roll solution exhibits similar behavior, with considerable fluctuation (the roll also shows this behavior because the FSS does not directly measure the roll as the IR sensor does). The final roll values are 1.64, 1.63, 0.7 degrees for the additive, multiplicative, and batch algorithms, respectively. The pitch shows a slightly more nominal behavior. Figure 6c shows the additive gyro bias estimates. The multiplicative gyro bias estimates look the same with final x, y, and z values of -5.786, -0.582, and -26.219 deg/hr. The batch again gives a much better estimate of gyro bias for z than the filters do. The gyro bias z solutions for the filters are better before the loss of the FSS. Near 750 seconds, the multiplicative gives a gyro bias solution of -1.3, 1.7, 1.3 deg/hour. The additive filter is similar. Once the FSS is lost, though, the filter is relying solely on the magnetometer. The residuals in this case are similar to previous results.

As in the case of the IR/MAG solutions, an attempt was made to stabilize the gyro bias estimation by increasing the measurement noise on the magnetometer from 3 to 50 milliGauss. Figure 6.d shows this result for the additive filter (the multiplicative filter is similar). In this case, the gyro bias is improved by increasing the magnetometer measurement noise. The final results are much closer to the actual values. The x gyro bias estimate is now better than the batch estimate. This technique may work better in the FSS/MAG combination since the FSS gives some estimate of the yaw solution, and thus the problem of relying only on the magnetometer for yaw estimation is avoided.

As in the case of the IR/MAG solutions, without the estimation of gyro bias the filters converge from much larger initial attitude errors. The yaw solutions are shown in Figures 6e and 6f for the additive and the batch. The multiplicative is similar with a final yaw of -0.647 degrees. The roll solutions converge to final values of 1.94, 1.19, and 0.46 degrees for the additive, multiplicative, and batch algorithms, respectively. The pitch solutions show a nominal behavior. For the additive filter a 50 degree initial attitude error was used, for the multiplicative and the batch algorithms the maximum initial attitude error was 30 degrees. The solutions converge quickly and the three algorithms give similar solutions.

The final two cases investigate the use of only one sensor. Figures 7a and 7b show the multiplicative EKF and the batch yaw solutions using only magnetometer data. The additive EKF yaw solution is similar to the multiplicative with a final value of -1.254 degrees. The a priori attitude error was set at 50 degrees and gyro bias was not estimated. All three converge to less than 1 degree (the additive eventually converges this far as well) error using approximately a half orbit of data. The pitch and roll solutions show similar results with the pitch solution converging within approximately 300 seconds. Figure 8 shows the yaw solution from the multiplicative filter using only IR data. The additive filter and batch algorithm did not converge using only IR data with an initial attitude error of 50 degrees. Figure 8 shows that the yaw solution eventually converges with only IR data due to quarter orbit coupling (related to the geometry of the ERBS attitude). The pitch and roll solutions converge within 10 seconds to values less than 0.05 degrees.

Sensor Calibration

A further test of gyro bias estimation was performed to determine if the filter could follow a change in the bias. In this case the gyro bias was started at 3.6 deg/hour on all axes, and after 300 seconds it was switched to -3.6 deg/hour. Figure 9 shows the estimation of this gyro bias by the additive filter. The filter follows the change and converges again within 200 seconds. The multiplicative filter exhibits similar behavior. The batch algorithm cannot estimate a gyro bias change since it estimates only a single solution at the epoch (and then the epoch attitude is propagated using the gyro data corrected for the epoch gyro bias).

The remaining calibration study focuses on the FSS, IR, and magnetometer. The same clean simulated data were used and biases were applied to the sensors being studied. A priori covariances were selected to be $1x10^{-7}$ (units for particular bias) for biases based on the sensitivity study performed on the gyro bias. In the future, sensitivity studies should be performed on each sensor calibration to determine the best a priori covariance. The first studies involved applying a single calibration error to only one sensor at a time. Several calibration errors were then applied to study the capability of the filters to estimate several

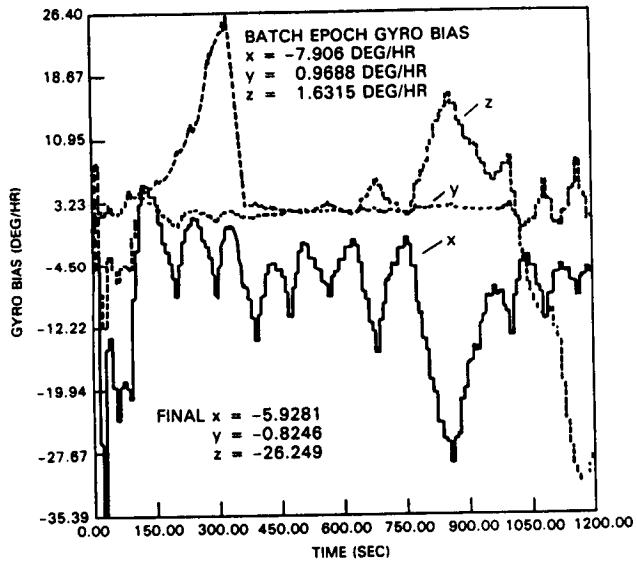

6c - GYRO BIAS, ADDITIVE

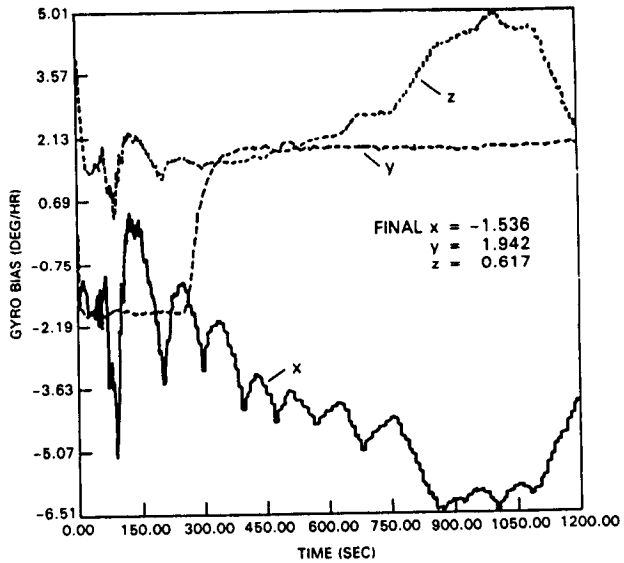

6d - GYRO BIAS, ADDITIVE (σ_{mag} = 50 mG)

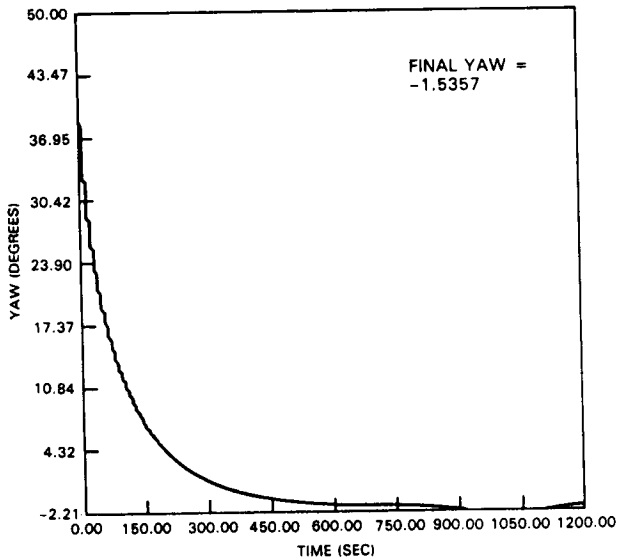

6e - YAW, ADDITIVE APRIORI ATTITUDE = 50 DEG)
(NO GYRO BIAS)

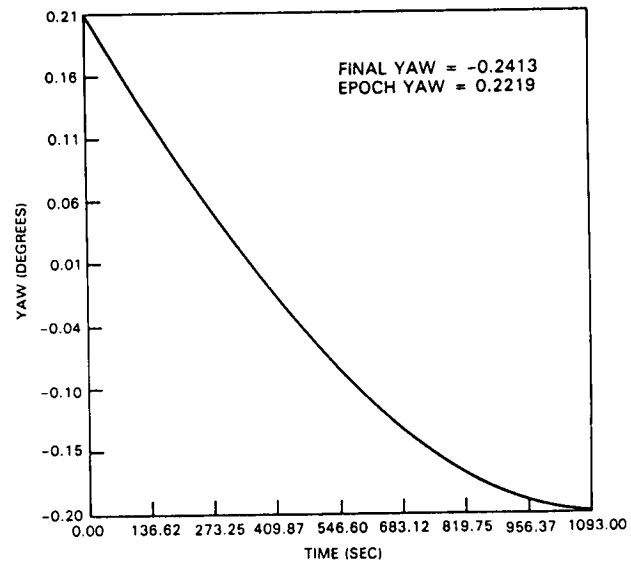

6f - YAW, BATCH (APRIORI ATTITUDE = 30 DEG)
(NO GYRO BIAS)

FIGURE 6. FSS/MAG SOLUTIONS

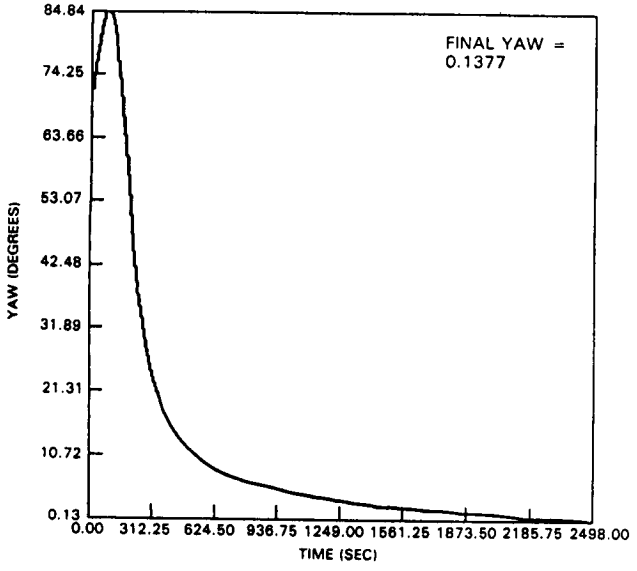

7a - YAW, MULTIPLICATIVE

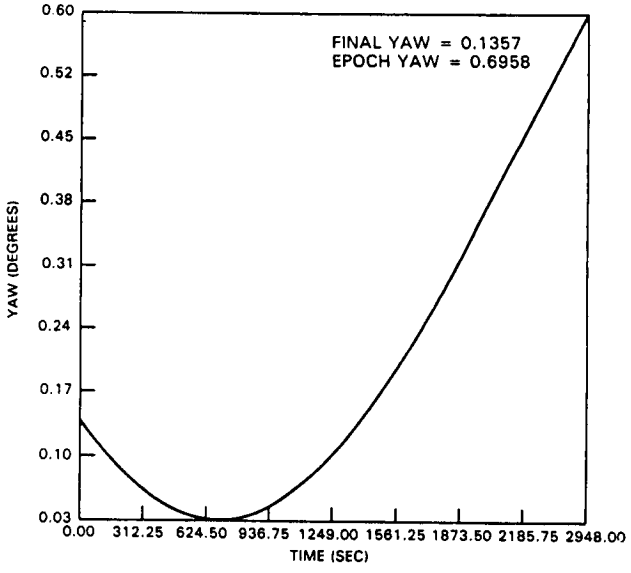

7b - YAW, BATCH

FIGURE 7. MAGNETOMETER ONLY (APRIORI ATTITUDE = 50 DEG)

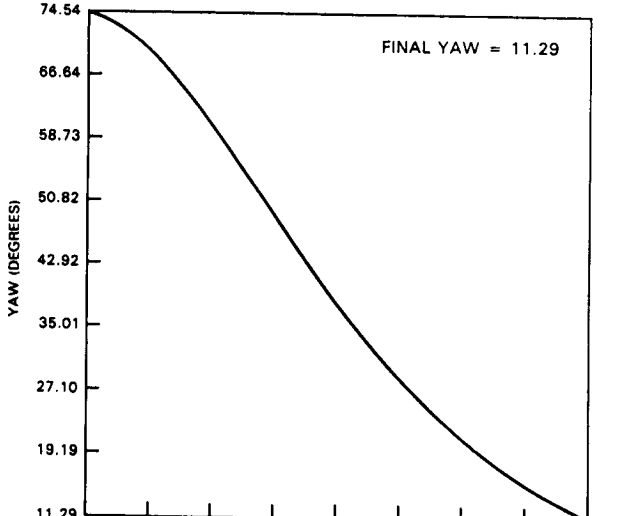

FIGURE 8. IR ONLY, MULTIPLICATIVE
(APRIORI ATTITUDE = 50 DEG)
(NO GYRO BIAS)

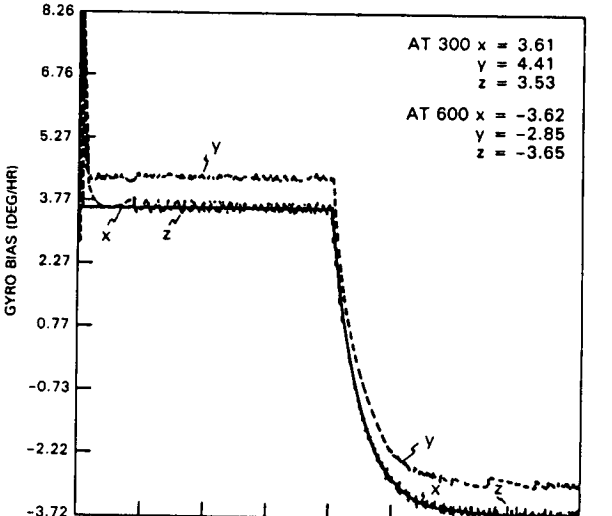

FIGURE 9. CHANGING GYRO BIAS ADDITIVE
(APRIORI ATTITUDE = 0 DEG)

calibration parameters at once.

The first calibration parameter to be studied was the IR bias. Table 3 shows the IR bias for the multiplicative and additive filters. The final entry in the table is the highest correlation coefficient, indicating the least observable component. A 0.1 degree bias was applied to both the measured pitch and roll. Table 3 shows that the multiplicative filter estimates the pitch bias quite well. The roll bias in the multiplicative filter is not observable. It is highly correlated with the first angle in the error state vector due to the geometry in this case. The FSS does not supply enough roll information. With

Table 3. Estimation of IR Horizon Scanner Pitch and Roll Bias (A priori attitude = 0 degrees)

		Bias (deg)		Uncertainty (deg)		Highest
Filter	Length	Roll	Pitch	Roll	Pitch	Correlation
Mult.	200 sec	-0.177	0.103	0.014	0.0006	$(\Theta_1,r)=0.989$
Add.	200 sec	-50.01	3.528	0.003	0.0105	all high

different geometry (the sun in a different location in the FOV or sun in the other FSS) the roll bias should be estimated as well as the pitch bias in the present example. The additive filter does not estimate either the pitch or roll bias well.

The next bias studied was an FSS bias. Table 4 shows the estimated values when a 0.1 degree bias was applied.

Table 4. Estimation of FSS Alpha and Beta Bias (A priori attitude = 0 degrees)

		Bias (deg)		Uncertainty (deg)		Highest
Filter	Length	alpha	beta	alpha	beta	Correlation
Mult.	200 sec	0.208	0.110	0.012	0.0011	$(\Theta_1,\alpha)=0.986$, $(\Theta_3,\alpha)=0.982$
Add.	200 sec	53.38	124.3	0.0005	0.0001	$(q_1,\alpha)=0.873$

Again the multiplicative filter estimated one of the biases (beta) quite well. With a longer run, the beta bias converges to approximately 0.1 degrees. The alpha bias is not observable again due to geometry. The additive filter shows poor estimation without significant observability problems as reflected by the correlation matrix.

The next bias estimated was magnetometer bias. A 10 milliGauss bias was applied on all axes. Table 5 shows that both filters estimate the bias quite well.

Table 5. Estimation of Magnetometer X, Y, and Z Biases (A priori attitude = 10 degrees, gyro bias estimated)

		Bias (mG)			Uncertainty (mG)			Highest
Filter	Length	X	Y	Z	X	Y	Z	Correlation
Mult.	200 sec	13.46	12.87	13.68	0.173	0.173	0.173	small
Add.	200 sec	13.48	12.90	13.72	0.173	0.173	0.173	small

The correlations were all very small. The estimated biases are all within 6 milliGauss (the resolution of the magnetometer) of the applied biases.

FSS misalignment was the final calibration error studied with the multiplicative filter. (The additive filter was not studied because of its poor performance estimating the previous calibration errors.) A 0.1 degree misalignment was applied to the FSS x and y axes and a 0.05 degree misalignment was applied to the FSS z axis. The misalignment uncertainty was 0.18 degrees. After 200 seconds the estimated misalignments were -0.070, -0.22, -0.51 degrees for the FSS x, y, and z axes, respectively, with uncertainties of 0.032, 0.043, and 0.093 degrees. The x and z misalignments are highly correlated to one another (the correlation coefficient was 0.998) but the three misalignments are not highly correlated to the attitude. Next, the filter was run with the same misalignments applied, but alpha and beta biases were solved for instead of

misalignments. This revealed that the filter could not distinguish the misalignments from biases. The beta bias, which corresponds to a y misalignment, was estimated well but the alpha bias was not since it is not observable at this attitude (this means that the x and z misalignments are also not observable). The estimated biases after 200 and 400 seconds were

$\alpha = 0.12 \quad \beta = 0.09 \quad \sigma = 0.005$ degrees (200 seconds)
$\alpha = -0.01 \quad \beta = 0.09 \quad \sigma = 0.0006$ degrees (400 seconds)

Data from different attitudes would be necessary to estimate the alpha bias and also to try and estimate the misalignments and distinguish them from biases.

The multiplicative filter was set up to solve for several calibration errors in one run. The estimated components consisted of attitude, gyro bias, FSS y misalignment, FSS beta bias, IR pitch bias, and magnetometer bias. The sensor errors applied were the same as those used previously. After 400 seconds the filter gave estimates of gyro and magnetometer bias like those given above (in the nominal cases). The filter did not give good estimates of the other calibration errors. With all the errors combined the FSS y misalignment and beta bias and the IR pitch bias were not observable, even though the beta and pitch biases were observable to the filter when applied alone. The geometry in this case does not give enough information to solve for all the parameters together. Again, data from several attitudes should be used and perhaps the state should be kept smaller when performing sensor calibration. It would be necessary to iterate to solve for all the sensor errors.

The gyro scale factor and misalignments were not estimated because a single attitude would not give sufficient observability. Attitude maneuvers would be necessary. This is also true for the FSS scale factor. The magnetometer misalignment or scale factors were not estimated in this initial study as they are likely not to be observable with the coarse ERBS magnetometer data.

Real Data

The last test studies the behavior of the filters when using real ERBS data. The orbit of data selected contained approximately 10 minutes of FSS data at the beginning and end of the orbit. Figures 10a and 10b show the multiplicative EKF and the batch algorithm estimates of yaw. The additive EKF yaw solution looks like the multiplicative with the same final value. Figure 10c shows the multiplicative gyro bias estimates. The additive has final x, y, and z gyro bias estimates of -7.393, -4.795, and 1.627 deg/hr, respectively. The roll and pitch solutions look similar to the yaw solution with final values of 0.07, 0.07, 0.10 degrees roll and 0.30, 0.30, 0.30 degrees pitch for the additive, multiplicative, and batch algorithms, respectively. The filters have slightly smaller estimates of yaw, and the three algorithms have similar values for pitch and roll. The gyro bias estimates are similar in y, but x and z are somewhat smaller for the two filters than for the batch (comparing the final filter results with the batch epoch). The two filters exhibit very similar behavior. The residuals for the FSS were considerably smaller for the two filters than for the batch algorithm. The IR residuals were similar and the magnetometer residuals exhibited behavior similar to that shown in Figure 5.d. In the case of the real data, the true reference is not known. The smaller residuals in the filters tend to give those solutions more credibility.

VIII. POTENTIAL APPLICATION

A version of the additive filter was created in which only attitude and gyro bias are solved for (the dimension of Equation 2.9 was reduced to 7). This filter was then tested with simulated ERBS data in a real-time attitude determination system (Reference 5). The filter was able to process the data and generate the attitude and gyro bias solutions shown in Figures 1 and 2 (baseline) in real time (the nominal ERBS data rate is 1 set of measurements every second). Currently, real-time attitude support in the Flight Dynamics Division is performed with single-frame estimators that solve only for attitude. The real-time filter has the capability of giving much more accurate solutions in a relatively short period of time (see Figures 1 and 2 for the length of time to converge). Gyro bias estimates could also be generated when sufficient data coverage is available. This real-time filter gives results comparable to the ERBS batch algorithm, which requires considerably more processing time and memory. This real-time filter is currently being adapted as a prototype system to be used by the GRO. Future missions, such as the SMEX series, are also planning to

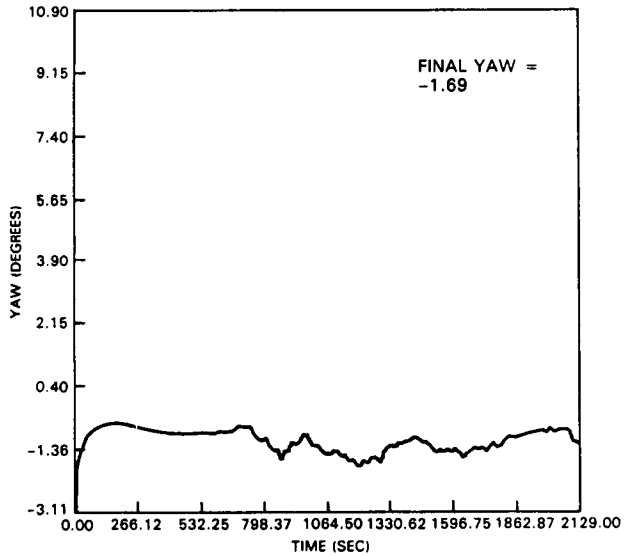

10a - YAW, MULTIPLICATIVE

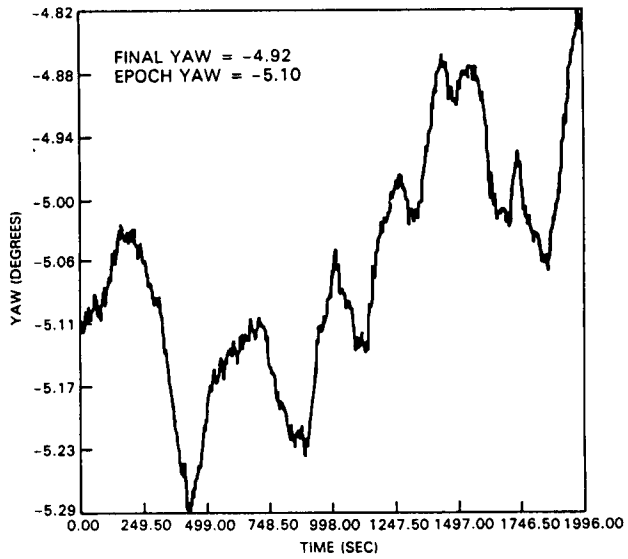

10b - YAW, BATCH

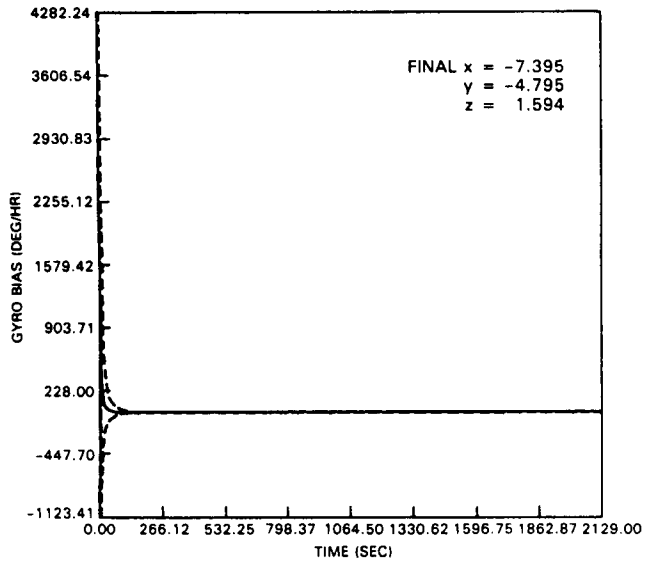

10c - GYRO BIAS, MULTIPLICATIVE

FIGURE 10. REAL DATA
(APRIORI ATTITUDE = 10 DEG)

BATCH EPOCH GYRO BIAS
x = -25.903 DEG/HR
y = -4.408 DEG/HR
z = -3.774 DEG/HR

implement a real-time filter, based on that developed for ERBS.

The full-state filter has potential application for non-real-time support. The initial test results given in Section VII demonstrate that it can give solutions comparable to the batch algorithm (in certain scenarios, others need further investigation as to why the filter solutions differ from the batch). It is also advantageous to combine the attitude estimation with the sensor calibration since the correlation matrix provides valuable information on observability conditions. The combined attitude determination and sensor calibration can be implemented into a batch algorithm. The batch algorithm, though, requires much more memory and has no means of compensating for dynamic noise which can affect an epoch attitude solution propagated over a long period of time.

IX. CONCLUSIONS

In the scenarios presented (using nominal simulated data) both filters, the additive and multiplicative, are very robust in attitude estimation. The filters can be started with large initial errors and still have quick convergence. The batch algorithm is more sensitive to large initial attitude errors in some cases. The filters also exhibit good estimation of gyro bias (when the optimal sensor data are available), although the batch converges with less data. The filters follow changes in attitude and gyro bias closely; the batch algorithm also follows an attitude maneuver closely but it cannot follow changes in gyro bias. When the optimal sensor combinations are not available, the filters must rely on the magnetometer data. The attitude solutions are still estimated well, but the gyro bias is not estimated as well. For ERBS this is a result of the coarseness of the magnetometer data. The batch algorithm does a better job estimating gyro bias in these cases. Further investigation into the weighting is necessary to find ways of improving the filter results (the results would also be improved with a more accurate magnetometer). Both filters also gave reasonable results when using real ERBS data. The filters had slightly smaller residuals than the batch algorithm. Since the true solution is not known, the residuals are the only real figure of merit.

The pseudo-measurement normalization technique is an acceptable normalization method when computer processing time is not critical. When the noise level is selected properly, the pseudo-measurement technique gives results comparable to the original normalization technique. When the noise level is not selected properly, the attitude solutions converge to the wrong value. In the scenario presented this had a significant impact on the pitch solution.

The multiplicative filter has better sensor calibration characteristics than the additive filter. The reasons why are not clear as of this writing. Perhaps the attitude singularity in the additive filter has an affect on the ability of that filter to distinguish and estimate sensor errors. With a single set of data, many calibration errors are not observable. Further study of the sensor calibration with different data spans, giving different sensor coverage, is necessary to fully determine the capabilities of the multiplicative filter. Additional studies should also be performed with sensor corruption, such as noise and data dropout.

REFERENCES

1. Deutschmann, J., and Bar-Itzhack, I.Y., "Extended Kalman Filter for Attitude Estimation of the Earth Radiation Budget Satellite", Flight Mechanics/Estimation Theory Symposium, NASA Conference Publication 3050, May 23-24, 1989

2. Bar-Itzhack, I.Y., and Harman, R.R., "True Covariance Simulation of the EUVE Update FIlter", Flight Mechanics/Estimation Theory Symposium, NASA Conference Publication 3050, May 23-24, 1989

3. Bar-Itzhack, I.Y., and Oshman, Y., "Recursive Attitude Determination from Vector Observations: Quaternion Estimation", IEEE Transactions on Aerospace and Electronic Systems, Vol. AES-21, Jan. 1985, pp.128-136

4. Gelb, A. (ed.), Applied Optimal Estimation, M.I.T. Press, Cambridge, MA 1988

5. Rokni, M., and Deutschmann, J., "Attitude Determination A Prototype Real Time Sequential Filter (RTSF) Evaluation Report", CSC/TM-90/6050, February 1990